Journal of The Electrochemical Society, **154** (12) B1305-B1314 (2007)
0013-4651/2007/154(12)/B1305/10/$20.00 © The Electrochemical Society

Validated Leverett Approach for Multiphase Flow in PEFC Diffusion Media

II. Compression Effect

E. C. Kumbur,* K. V. Sharp, and M. M. Mench,z**

Fuel Cell Dynamics and Diagnostics Laboratory, Department of Mechanical and Nuclear Engineering, The Pennsylvania State University, University Park, Pennsylvania 16802, USA

This work is the second part of a series of papers to describe the multiphase transport mechanism in thin-film polymer electrolyte fuel cell (PEFC) diffusion media (DM). The present work is devoted to delineating the effects of compression. Direct measurements of drainage capillary pressure-saturation curves for SGL series carbon paper DM tailored with a range of mixed wettability were performed at room temperature under various compressions (0, 0.6, and 1.4 MPa) typically encountered in a fuel cell assembly. Based on these benchmark data, an appropriate form of the Leverett approach, including a Leverett-type empirical function that incorporates the effect of compression and the mixed wettability characteristics of the tested DM samples, was developed. The presented approach can determine the capillary pressure as a function of hydrophobic additive content, liquid saturation, compression, and uncompressed porosity of the DM. Compression leads to an increase in capillary pressure, effectively caused by the corresponding reduction in effective porosity. Any increase in hydrophobicity amplifies the compression effect, yielding a higher capillary pressure for the same saturation level. Furthermore, the fraction of connected hydrophilic pores is observed to be reduced with an increase in compression, leading to a favorable reduction in water storage capacity of the fuel cell DM.
 [DOI: 10.1149/1.2784285]

Manuscript submitted March 28, 2007; revised manuscript received August 10, 2007. Available electronically October 16, 2007.

Proper tailoring of the water management in polymer electrolyte fuel cells (PEFCs) has the potential to significantly increase stack power density, durability, and performance stability while decreasing freeze/thaw damage and transient response time. Quantification of the multiphase transport characteristics of the thin-film diffusion media (DM) has come to the forefront as a key step in establishing the most favorable microfluidic strategy that can balance the flooding effects (limiting the oxygen transport to the catalyst layer) and the membrane drying phenomena (loss of proton conductivity) in an operational cell. However, achieving an optimal balance is challenging because of the extremely complex internal architecture of the fuel cell DM with mixed wettability and the strong interaction of transport properties with the operational conditions.[1,2]

The bimodal pore distribution and the mixed wettability characteristics of the DM greatly influence the multiphase flow within the pores of the DM.[1] Accurate multiphase transport characterization of such thin-film media requires an appropriate capillary pressure-liquid saturation relationship that is fundamentally dependent on material properties and operating conditions, including but not necessarily limited to poly(tetrafluoroethylene) (PTFE) content, pore size, compression, and temperature. However, a complete understanding of the multiphase flow in these unique media has not yet been well established, and the basic tools used to correlate the governing transport parameters are borrowed from soil science. The empirical transport models adopted from soil science are based on experiments performed for different types of soils having uniform wettability. Hence, they are well-suited for characterizing the transport in those types of porous media. Because of the structural difference between the soils for which these approaches originated and the fuel cell DM, these approaches are not fully capable of accurately representing the capillary transport within the pores of the fuel cell DM tailored with mixed wettability. A so-called semiempirical Leverett approach[3] equipped with the standard Leverett *J*-function (proposed by Udell[4]) is considered a common tool to characterize the liquid transport in a range of unconsolidated soils with uniform wettability. In terms of modeling the capillary transport in fuel cell DM, the calibrated version of the traditional Leverett approach proposed for hydrophobic fuel cell DM by Pasaogullari and Wang[5] and Nam and Kaviany[6] has commonly been employed to simulate the liquid transport and determine the governing capillary transport parameters within the fuel cell DM. Although the usefulness and merits of the Leverett approach are clear, this traditional approach in its original form has been shown to have some major limitations in accurately describing flow through these highly complex heterogeneous media.[1,7] Because of the apparent limitations of this approach, existing models are limited in the provision of qualitative guidance for the design of next-generation fuel cell materials; therefore, a higher level of precision is now required.

Proper stack assembly requires careful integration of components with an optimum assembly pressure to prevent leakage and assure a proper contact surface from the lands to the DM.[8] Typically, low compression in a fuel cell stack assembly causes an increase in gas leakage and electrical contact resistance, leading to poor performance, while overcompression of the DM leads to an irreversible deformation in DM structure.[9,10] Thus, optimization of the assembly pressure is of great importance.[8,11,12] Furthermore, depending upon the size of the components in the stack, the DM may experience various compression loadings, generating strong local stresses that can alter the morphological structure and the multiphase transport characteristics of the DM. It has been established that for a given thin-film fuel cell DM, any compression is followed by a decrease in porosity and an increase in tortuosity.[13-15] In addition, the discontinuity of the surface contact area at the DM–flow channel interface creates inhomogeneous compression distributions, yielding substantial changes in local physical properties of the DM.[9,10] The portion of the DM in contact with the landings is subjected to higher compression, whereas the portion under the flow channel experiences less compression and tends to intrude into flow channels, thus resulting in increased reactant flow-field pressure drop.[16] The axial variation of the compression in the cell assembly yields discrete regions that have different capillary transport characteristics. Furthermore, the non-uniform change of the surface area and the pore size in these discrete regions is reasonably expected to change the behavior of multiphase flow, yielding discrete transport patterns between the channel and land locations. Therefore, it is necessary to quantify the degree of change in capillary transport characteristics of a DM under different compression loadings.

Much literature is devoted to examining the effects of the stack assembly pressure on cell performance,[8,12,17,18] but the changes in the capillary transport characteristics of a DM have not been explicitly addressed. The change in spatial variation of the pressure was

* Electrochemical Society Student Member.
** Electrochemical Society Active Member.
z E-mail: mmm124@psu.edu

Table I. Material properties of the tested DM samples.[a]

Material	Type	Thickness (μm)	PTFE Macro-substrate (wt %)	Uncompressed porosity	Permeability (cm^3/cm^2 s)
SGL 24BC	Paper w/MPL	235	5	0.76	0.60
SGL 24DC	Paper w/MPL	235	20	0.75	0.45
SGL 10BB	Paper w/MPL	420	5	0.84	3.00

[a] All values are adapted from manufacturer technical specification sheets. Note that the values of porosity, permeability, and PTFE content given above represent the material properties of the tested macro fuel cell diffusion media substrate (i.e., macro DM without MPL).

modeled under varying compression pressures,[9,10] and the corresponding reduction in local porosity was qualitatively coupled with the local current density distribution by Lee et al.[17] The fluctuation in current density profile due to varying compressions is believed to be an indicator of the existence of the mass-transport resistance.[12] Recently, Bazylak et al.[11] analyzed scanning electron microscope (SEM) images of the compressed DM and reported that the fiber breakage due to the compression leads to a decrease in flow resistance. The decrease in flow resistance is qualitatively attributed to the possible loss of hydrophobicity. The existing studies provide insightful background, but to the best of the authors' knowledge, no truly direct study elucidating the effect of cell assembly pressure on the capillary transport characteristics of a fuel cell DM has been reported.

This work is the second part of a series of papers describing the directly measured multiphase transport characteristics of the SGL series carbon paper DMs with various degrees of mixed wettability (from 5 to 20 wt %) over a range of realistic compression loadings (0, 0.6, and 1.4 MPa). Based on the experimental measurements, we present an updated version of the Leverett approach appropriate for the tested DM samples that incorporates the compression effect and accounts for the mixed wettability characteristics of the tested DM samples through a Leverett-type empirical function presented in the first part of this paper series.[19] This alternative approach can precisely determine the capillary pressure as a function of hydrophobic additive content, liquid saturation, compression pressure, and uncompressed porosity of the DM within the limits of the tested parameters. The succeeding publication[20] addresses the effect of operating temperature on the capillary transport characteristics of the fuel cell DM and its incorporation into the version of the Leverett approach presented in this study.

Method of Approach

SGL 24 series (SIGRACET diffusion media) and SGL 10BB nonwoven carbon papers were investigated in the present study. The material properties of tested DM samples are provided in Table I for convenience. The selected DM samples are coated with a microporous layer (MPL), which is composed of carbon black powder and hydrophobic agent called PTFE. The major aim of introducing the MPL on the cathode is to provide better electrical contact with the adjacent component and alleviate the flooding effects. These selected DM samples are treated with PTFE (hydrophobic agent) from 5 to 20 wt %, which is in a typical hydrophobic treatment range preferred in conventional fuel cell applications.

The method of standard porosimetry (MSP), developed by Porotech, Ltd., was employed to measure the desired transport parameters in thin-film DMs. MSP provides a means of nondestructive testing for investigation of any type of porous materials, including soft, frail materials and powders.[21] The experimental approach and the detailed description of the MSP technique are provided in Ref. 19 and 21, respectively. This technique is based on the capillary equilibrium principle and capable of performing measurements in a wide range of pore sizes, from 10^6 to 3×10^6 nm in multicomponent porous materials. One distinct advantage of MSP over the conventionally used method of mercury porosimetry (MMP) is that MSP does not require the high pressures (up to thousands of atmospheres) that can lead to a substantial structural deformation of the tested porous materials in MMP.[21] A more detailed discussion of MSP vs MMP is provided in Ref. 21.

The current MSP experiments were performed at fixed levels of compression, i.e., 0, 0.6, and 1.4 MPa, providing data on both the structural changes and the corresponding transport properties of the DM samples. The DM samples were sandwiched between the two standard samples having the same size of tested DM specimens to ensure a uniform compression on the samples. Additional compressive strain-stress experiments were also performed using a highly sensitive compression gauge to provide data on the elasticity behavior of the tested DM samples.

Results and Discussion

Effect of compression on morphological characteristics.— Any fluid displacement across a porous medium is usually more closely associated with the intricate pore morphology rather than the fluid properties.[21] The specific pore structure and the mixed wettability characteristics of the DM are strongly coupled with the compression strain, because any change in the electrode structure (including DM) can cause a substantial change in the multiphase transport characteristics. In that sense, the investigation of the changes in the morphological structure of the porous DM as a function of assembly compression is critical to establishing the accurate multiphase transport characteristics of the fuel cell DM.

Pore characteristics.— The DM samples were subjected to compression loadings of 0, 0.6, and 1.4 MPa to isolate the effects of compression on the pore network characteristics. Total (hydrophilic and hydrophobic) pore distributions for SGL 24BC and SGL 24DC under different compressions (0 and 1.4 MPa) are shown in Fig. 1. For a given DM, the pore network follows a similar qualitative pattern under the influence of compression; however, the corresponding pore size distribution shifts to smaller values with increasing compression. For the tested SGL 24 series DM samples, the average pore radius of the total pore network is found to be higher under no compression (4.8 μm for SGL 24BC and 3.9 μm for SGL 24DC), whereas the highest compression (1.4 MPa) yields a smaller average pore radius (3.5 μm for SGL 24BC and 3.1 μm for SGL 24DC). The average pore radius of DM samples corresponding to all different compressions tested is shown in Table II.

The pore characteristics of the individual components (macro- and microsubstrates) were investigated by means of the pore-distribution data of the tested DM samples, as described in Ref. 19, to identify the relative significance of the morphological changes in different layers of the bilayered DM (i.e., MPL and macro-DM substrate). As seen from Fig. 1, the pore space of macroporous substrate (pore radius >1 μm) seems to be more affected by the compression, thereby exhibiting a greater reduction in pore volume than that of the microporous layer (pore radius from 0.01 to 0.1 μm). This can be attributed to the fact that the compact composition of the MPL provides an initially lower surface area and pore volume, yielding a more rigid structure. This feature, in turn, improves the elasticity of the MPL and results in less strain (less deformation) under the compression than that of macroporous substrate. As a result, any force exerted on the DM samples is mostly absorbed by the *macro*-substrate.

Surface area.— The specific surface area of a DM is also a particularly important macroscale parameter. Any change in interfacial surface area available for mass transport can affect the microscale distribution of fluids inside the DM. The total (hydrophilic and hydrophobic) specific surface area under the compression of 0, 0.6, and 1.4 MPa for SGL 24BC and SGL 24DC was measured and is shown in Fig. 2. As seen in Fig. 2, for both DM samples, applying

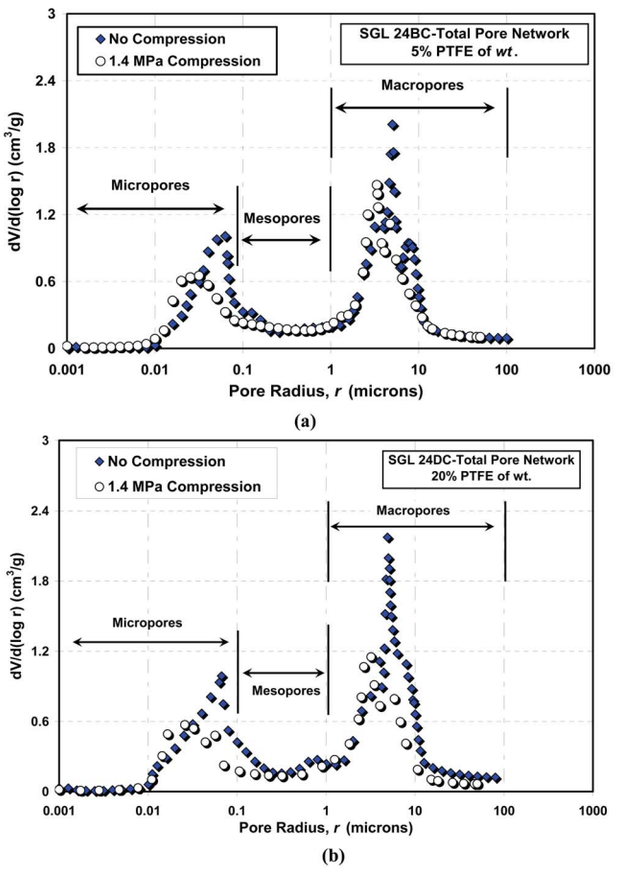

Figure 1. (Color online) Dual (hydrophobic and hydrophilic) pore distribution under 0 and 1.4 MPa compression of (a) SGL 24BC and (b) SGL 24DC carbon paper.

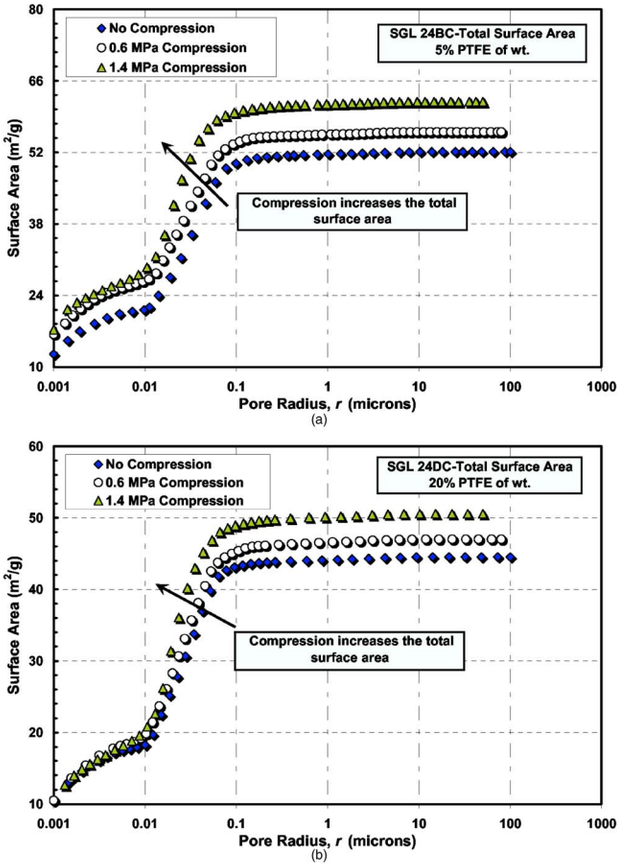

Figure 2. (Color online) Total (hydrophobic and hydrophilic) surface area under 0, 0.6, and 1.4 MPa compression of (a) SGL 24BC and (b) SGL 24DC carbon paper.

compression reduces the pore volume (radius from 0.001 to 0.1 μm) and increases the interfacial surface area, thus distorting the available transport pathways and increasing the tortuosity. The available void space for the transport of the species within the pore matrix of the DM is also highly sensitive to any change in the effective stress applied on the DM, which is also a strong function of compression. Applying compression on the DM can change the void ratio (i.e., decreasing the void volume), thus reducing the permeability for the transport. Therefore, the decrease in effective porosity is accompanied by a reduction in permeability, which in turn restricts the liquid flow and causes a higher mass (liquid and gas phase) transport resistance.

The effect of thickness.— The present results also suggest that the thickness of the bilayer DM influences the compression characteristics and its corresponding effects on the pore structure. One distinctive observation drawn from these measurements is that SGL 10BB (420 μm) exhibits a considerable increase in the total pore surface area with regard to the increase of compression. Figure 3 shows the total (hydrophilic and hydrophobic) surface area of SGL 10BB under 0.6 and 1.4 MPa compression. The increase in total surface area of SGL 10BB, especially in the meso- and microporous components (pore radius <0.1 μm), is more pronounced at 1.4 MPa compression than that of SGL 24 series (SGL 24BC, 24CC, and 24DC). Recalling that SGL 10BB DM has a thickness of 420 μm (almost twice that of the SGL 24 series), the increase in bulk thickness of the DM appears to amplify the effect of compression on reduction in pore volume and causes an increase in interfacial surface area. The thinner DM (SGL 24 series), however, appear to be more resistive to deformation and can better sustain their pore characteristics under higher compression loadings due to the relatively more compact and rigid structure compared to the thicker DM. Thus, the compressive

Table II. Material properties of the tested DM determined by the MSP technique.

	Total porosity/hydrophilic porosity			Total surface area (m^2/cm^3)/ average pore radius (μm)		
Material	0 MPa	0.6 MPa	1.4 MPa	0 MPa	0.6 MPa	1.4 MPa
SGL 24BC (5% PTFE)	0.75/0.27	0.72/0.21	0.71/0.23	23.4/4.8	27.6/5.5	31.0/3.5
SGL 24DC (20% PTFE)	0.71/0.21	0.70/0.16	0.70/0.17	28.5/3.9	30.8/3.1	32.4/3.1
SGL 10BB (5% PTFE)	0.83/0.47	0.79/0.41	0.77/0.41	17.5/3.9	19.0/3.6	19.6/3.9

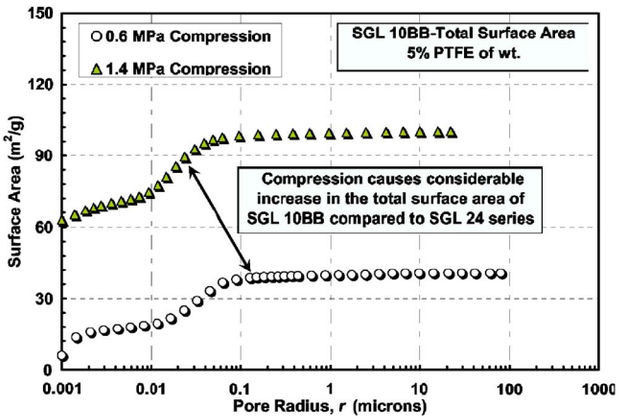

Figure 3. (Color online) Total (hydrophobic and hydrophilic) surface area of SGL 10BB carbon paper (with a thickness of 420 μm) under 0.6 and 1.4 MPa.

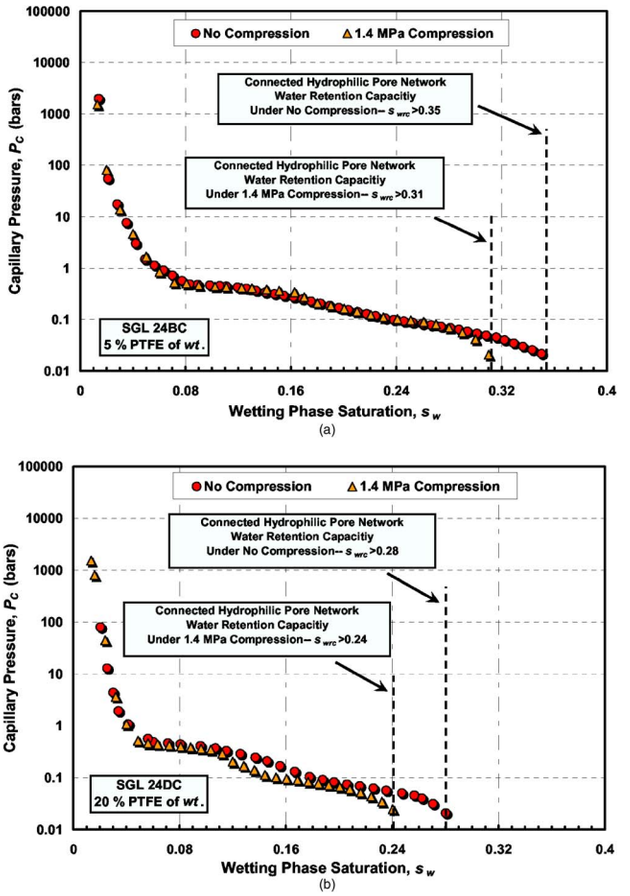

Figure 4. (Color online) Capillary pressure vs wetting phase saturation of the connected hydrophilic pore network under 0 and 1.4 MPa compression of (a) SGL 24BC and (b) SGL 24DC carbon paper.

strain characteristics of the DM and its effect on the capillary transport process should be included in attempts to accurately model the two-phase flow in the DM.

Water retention behavior and hydrophilic pore network.— The different DM morphologies exhibit a range of surface area to pore volume ratios, yielding different wetting phase configurations and immobile liquid saturations. The water retention characteristic (water storage capability) of a DM is an important parameter affecting the water storage behavior of the fuel cell DM. Neutron imaging studies by Mench and co-workers[22,23] have revealed that two different fuel cell configurations can have nearly identical performance but can yield large differences in the stored water content. At the stack level, the target of the designs is to reduce the stored water content in order to promote durability, mitigate freeze/thaw damages, and reduce the parasitic purge requirements. Motivated by these targets, it is desirable to find the best DM configuration that will promote low water retention. For that reason, the water retention behavior in different pore configurations needs to be thoroughly analyzed before an optimized structure can be proposed or complex models are complete.

Spontaneous capillary imbibition experiments were performed to determine the fraction of accessible connected hydrophilic pathways in the tested DM samples. The detailed description of experimental approach is outlined in our previous publication (Ref. 19) and in Ref. 21. The MSP technique provides a means for isolating the connected hydrophilic pore network from the total pore network by utilizing various liquids with different wettability.[21] The corresponding capillary pressure–liquid saturation of the connected hydrophilic pore network was obtained at various levels of compression. The measurement of the connected hydrophilic pore volume enables reasonable estimates of the water retention capacity (water storage) of the DM (s_{wrc}), which is, in fact, a measure of available hydrophilic pore space that can spontaneously imbibe and store liquid water in the DM.

Figure 4 represents the measured capillary pressure-wetting phase saturation relationships of the connected hydrophilic pore network (excluding the isolated pores) for SGL 24BC and SGL 24DC carbon paper under 0 and 1.4 MPa compression. The capillary pressure shown in Fig. 4 represents the spontaneous imbibition pressure. As seen in Fig. 4, the capillary pressure approaches zero as the DM imbibes the maximum water, meaning that once the threshold saturation is reached, no connected hydrophilic pore space is available for the DM to further imbibe water. From Fig. 4, the amount of water to fill the available connected hydrophilic sites is observed to decrease with compression. The amount of water imbibed in SGL 24BC (5 wt % PTFE) is reduced from 0.35 ($s_{wrc} > 0.35$) to 0.31 ($s_{wr} > 0.31$) as the compression is increased to 1.4 MPa. However, even though SGL 24DC (20 wt % PTFE) exhibits a similar decrease in response to increase in compression ($s_{wrc} > 0.28$ for no compression, $s_{wrc} > 0.24$ for 1.4 MPa compression), the compression yields different quantitative water retention capacities for the tested SGL 24 series DM samples due to the different PTFE loading. It is hypothesized that higher PTFE loading of the DM reduces the available hydrophilic pathways for the uncompressed[19] and to a certain extent compressed DM.

The results shown in Fig. 4a and b also suggest that the tested DM samples appear to preserve their relative wettability characteristics under high compressions (i.e., 1.4 MPa), because the results indicate that SGL 24BC treated with 5% PTFE imbibes to a maximum saturation of 0.35 ($s_{wrc} > 0.35$), whereas SGL 24DC tailored with 20% PTFE can only imbibe up to a maximum of 0.28 saturation ($s_{wrc} > 0.28$).

Effects of bulk thickness on the water retention characteristics of the DM were also investigated. Figure 5a shows the water retention behavior of SGL 10BB (5 wt % PTFE, with a thickness of 420 μm) under 0.6 and 1.4 MPa compression. The noticeable decrease in the amount of imbibed water in the hydrophilic sites of SGL 10BB DM sample as compared to SGL 24 series (235 μm) is clearly seen from Fig. 4 and 5a. At 0.6 MPa compression, the macro- and microporous substrate of SGL 10BB carbon paper can imbibe the water up to a maximum saturation of 0.56 ($s_{wrc} > 0.56$), meaning that the available pore space is almost equally shared by the hydrophilic and hydrophobic pores. However, as the compression pressure is further increased to 1.4 MPa, the connected hydrophilic pore volume re-

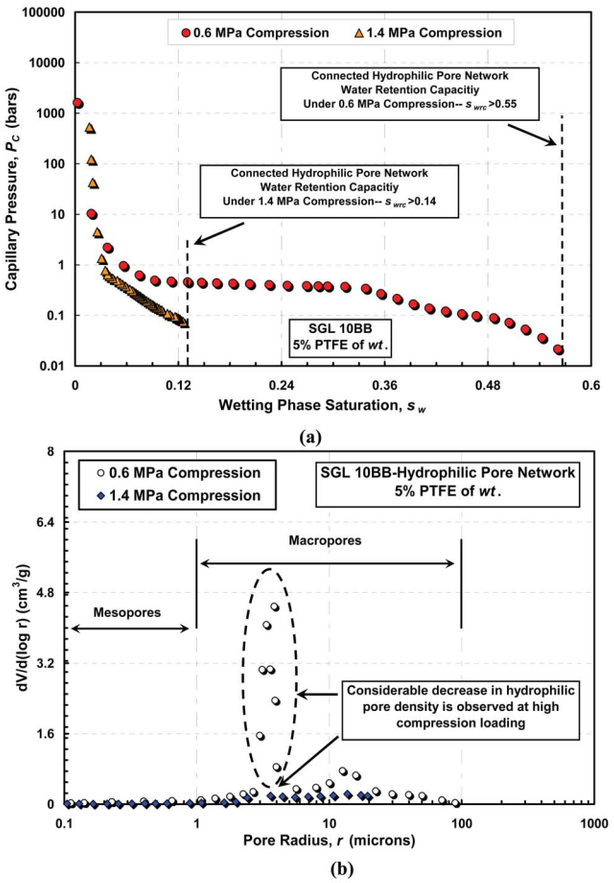

Figure 5. (Color online) (a) Capillary pressure-saturation for connected hydrophilic pore network of SGL 10BB under 0.6 and 1.4 MPa compression and (b) hydrophilic pore distribution of SGL 10BB under 0.6 and 1.4 MPa compression.

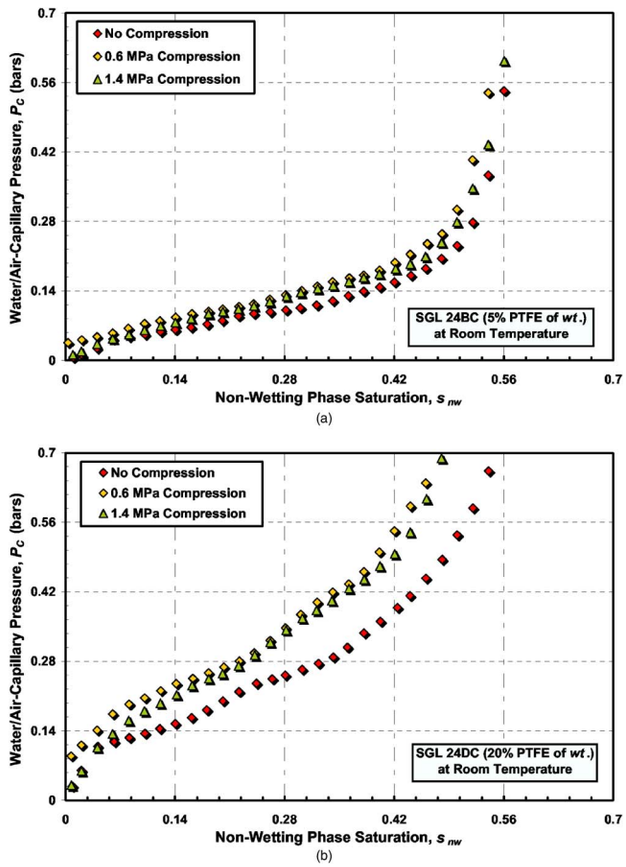

Figure 6. (Color online) Water/air capillary pressure vs nonwetting phase saturation of the total hydrophobic pore network under 0, 0.6, and 1.4 MPa compression of (a) SGL 24BC and (b) SGL 24DC carbon paper.

duces significantly, allowing maximum spontaneous imbibition of only 0.14 ($s_{wrc} > 0.14$). This significant change can be attributed to a larger reduction in connected hydrophilic pore space with increasing compression in this thicker DM sample (420 μm). The higher deformation of the thicker sample (SGL 10BB) results in decreasing available hydrophilic pore sites, limiting the imbibition of water. The substantial decrease in hydrophilic pore density due to the compression can also be observed from hydrophilic pore distribution shown in Fig. 5b. The measured hydrophilic porosity and the corresponding maximum imbibed water saturation are given in Tables II and III, respectively.

In summary, applying compression and increasing PTFE content promote a reduction in the connected hydrophilic pore volume and hence, in the water retention capacity of the DM (self-imbibed water content). From a fuel cell perspective, the reduction of stored water would provide better control of dynamic transport through thin-film DM, leading to improvement in both the steady and dynamic fuel cell performance, decreased startup time from frozen conditions, better purge capability, and enhanced durability.[22,23] The current results are consistent with those in the soil science literature, emphasizing the strong dependence of water retention ability on the spatial heterogeneity of the porous medium, the variation of physical material properties, and deformation of media itself.[24]

Table III. Water retention capacities of the tested DM samples under compression.

Material	PTFE content (wt %), thickness	Estimated water retention capacity 0 MPa	0.6 MPa	1.4 MPa
SGL 24BC	5%, 235 μm	$s_{wrc} > 0.35$	$s_{wrc} > 0.33$	$s_{wrc} > 0.31$
SGL 24DC	20%, 235 μm	$s_{wrc} > 0.28$	$s_{wrc} > 0.26$	$s_{wrc} > 0.24$
SGL 10BB	5%, 420 μm	$s_{wrc} > 0.58$	$s_{wrc} > 0.56$	$s_{wrc} > 0.12$

Capillary pressure-saturation curves.— The drainage curves of the air-water capillary system of the total hydrophobic pore network under the compression of 0, 0.6, and 1.4 MPa were obtained to delineate the effect of compression on the capillary-induced flow within the tested fuel cell DM samples. Figure 6 shows the total hydrophobic network nonwetting saturation vs air-water capillary pressure of SGL 24BC and SGL 24DC (both coated with MPL) subjected to compression of 0, 0.6, and 1.4 MPa. The individual curves follow similar qualitative trends, yielding slightly different quantitative values. The capillary pressure increases with an increase in nonwetting phase saturation at each compression condition, as expected for a PTFE-coated DM. The compression, shown to cause a decrease in the pore size (Fig. 5b), generally promotes a higher capillary pressure to overcome the increased surface energy of the distorted pores (Fig. 6), though there is little quantitative difference between the 0.6 and 1.4 MPa curves. The increase in capillary pressure of the hydrophobic pore network due to the reduced pore size can also be explained through the Young–Laplace theorem, which

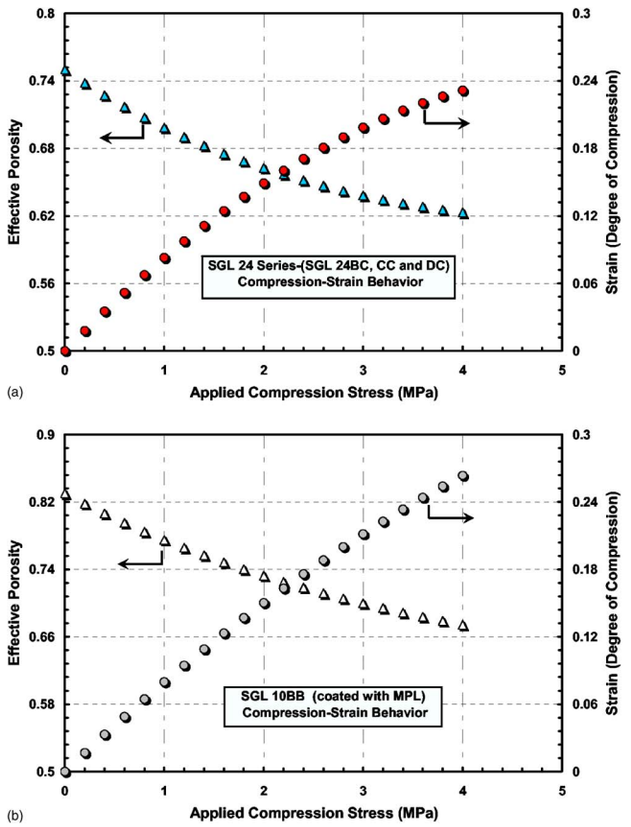

Figure 7. (Color online) Compressive strain and effective porosity vs applied compression pressure curves for (a) SGL 24 carbon paper series (SGL 24BC, CC, and DC) and (b) SGL 10BB carbon paper.

correlates the capillary pressure for a cylindrical pore in terms of pore radius, surface tension, and contact angle.[25] The Young–Laplace equation is given as

$$P_C = P_{nw} - P_w = \frac{2\gamma \cos\theta}{r} \quad [1]$$

where γ, θ, and r represent surface tension, contact angle, and pore radius, respectively. Compression exerted on the DM causes change in the morphological structure, decreasing the pore radius. The decrease in average pore radius leads to an increase in capillary pressure, as can also be seen in Eq. 1.

One other distinctive observation obtained from these measurements is that the increase in capillary pressure with compression is more pronounced between an uncompressed and 0.6 MPa compression condition (Fig. 6). However, any further increase from 0.6 to 1.4 MPa seems to have less effect on the measured capillary pressure, which holds true for all tested DMs. For SGL 24DC carbon paper DM, the measured capillary pressure increases with an average of 30.5% from 0 to 0.6 MPa, whereas there is almost no variation in the measured capillary pressures when the compression is further increased from 0.6 to 1.4 MPa.

Additional compressive strain-stress experiments were performed to create a link between the strain characteristics of the DM and the corresponding change in capillary pressure. The compressive strain vs the applied pressure for SGL 24 carbon paper series and SGL 10BB is shown in Fig. 7. The compressive strain is found to be sensitive, but not that sensitive, to changes in pressure, reaching a value of 0.20 at 3 MPa for SGL 24 series. The slight decrease in the slope of the strain-stress curve (Fig. 7) with increasing compression can be attributed to slight increase in stiffness of the DM with compression. As the DM is compressed, the available pore space reduces, affecting the capillary pressure within the pores. Recalling that the compressive strain governs the degree of the reduction in pore size, the substantial increase in capillary pressure within the range of compression from 0 to 0.6 MPa can be linked to the increase of strain rate (shown in Fig. 7), which leads to a higher reduction in pore size.

In terms of the relatively very slight change in the measured capillary pressure within the compression range from 0.6 to 1.4 MPa, the reduction in effective pore radius and the sensitivity of the wettability characteristics with compression must be analyzed together. The behavior of the measured capillary pressure within this compression range (from 0.6 to 1.4 MPa) can be attributed to the relatively higher increase of the hydrophilic surface area of the DM substrate with compression. In other words, any further increase in compression from 0.6 MPa seems to promote the dispersion of more hydrophilic sites, producing higher hydrophilic surface area, thus enhancing the hydrophilic characteristic of the DM. The decrease in the hydrophobicity of the DM with compression is also observed in the extensive SEM analysis performed by Bayzlak et al.[11] Based on the analysis of the SEM images, the compression is observed to manifest as irreversible damage to the DM structure, causing PTFE coating breakage on the fiber surface and locally producing more hydrophilic sites.

A validated Leverett approach.— Almost every multiphase transport model requires the specific capillary pressure-saturation relationship of fluid and porous medium to correlate the capillary pressure as a function of saturation, wettability, and other material properties. A traditional semiempirical approach applicable for homogenous water-wet sand with uniform wettability was proposed by Leverett.[3] Based on the experimental data provided by Leverett,[3] Udell[4] introduced the functional form of the Leverett *J*-function. In terms of fuel cell studies, the Udell and Leverett correlation was calibrated for hydrophobic DM by Pasaogullari and Wang[5] and Nam and Kaviany.[6] Currently, the following form of the original Leverett approach is the typically employed in the fuel cell modeling framework to estimate capillary pressure as a function of liquid saturation[19]

$$P_C = \gamma \cos\theta \left(\frac{\varepsilon}{k}\right)^{1/2} J(s)$$

$$J(s) = \begin{cases} 1.417(1-s) - 2.120(1-s)^2 + 1.263(1-s)^3 & \text{if } \theta < 90^\circ \\ 1.417s - 2.120s^2 + 1.263s^3 & \text{if } \theta > 90^\circ \end{cases} \quad [2]$$

Our previous study[1,19] suggests that the generic Leverett approach given in Eq. 2 is insufficient for describing the capillary transport characteristics of a mixed wettability fuel cell DM. A more complete approach would incorporate a wide range of macroscopic variables, such as the rate of change of wetting phase saturation, pore size, the wetted fraction of the solid surface, the specific solid interfacial area of the fuel cell DM, and operational conditions such as compression and temperature. The effect of PTFE content and mixed wettability characteristics of the DM has been thoroughly investigated and addressed in the first part of this paper series.[19] This article focuses on developing an updated version of this approach that also incorporates the specific effects of compression and mixed wettability. The effect of temperature and an overall unified approach are the subjects of the following paper.[20]

Herein, a form of capillary pressure-saturation equation (a Leverett-type approach) appropriate for the hydrophobic pore network of the tested fuel cell DMs was developed to accurately determine the capillary pressure as a function of liquid saturation, PTFE content, uncompressed porosity, and compression pressure of the DM. The present approach is capable of incorporating the necessary

adjustments corresponding to the changes in the transport parameters and the wettability characteristics of the DM. The procedure of our integrated approach is structured as follows.

The drainage capillary pressure measurements of the hydrophobic pore network for SGL 24 carbon paper series (described in previous sections) were compiled in an expanded database. The specific compressive strain-stress relationships measured for the tested DM samples were obtained to capture the deformation and the change in the effective porosity of the tested SGL 24 series DM samples. The corresponding reduction in pore size as a function of compression was precisely determined based on the measured and the given material properties. The effective porosity was precisely linked to the corresponding pore volume change and the degree of deformation (compressive strain). Subsequently, the nondimensional effective pore size parameter, $(k/\varepsilon)^{0.5}$, used in the traditional Leverett approach was calibrated to account for the changes in effective porosity of the tested DM samples due to the compression. Consequently, a general equation correlating the effective porosity (ε_c) as a function of compressive strain (s_{TR}) and uncompressed porosity (ε_o) was derived, based on measured data

$$\varepsilon_c = \left[\frac{0.9}{1 + s_{TR}} + 0.1\right]\varepsilon_o \quad [3]$$

Based on compressive strain-stress experiments, the compressive strain of the tested DM samples as a function of compression pressure is found as

$$s_{TR} = -0.0083C^2 + 0.0911C \quad \text{SGL 24 series carbon papers} \quad [4]$$

$$s_{TR} = -0.0046C^2 + 0.0843C \quad \text{SGL 10BB carbon paper} \quad [5]$$

where C represents the compression pressure (MPa). Note that the compressive strain-stress relation is a characteristic property of the DM and varies for different DM materials. The effective porosity vs applied compression stress (MPa) for SGL 24 series and SGL 10BB DM samples is also shown in Fig. 7. As the compression increases, the effective porosity and the permeability reduce for both DM types. The effective porosity of SGL 24 series and SGL 10BB is found to be 0.66 and 0.73 at a compression of 2 MPa and it reaches a lower value of 0.62 and 0.67 at 4 MPa, respectively.

Instead of the standard Leverett function $[J(s_{nw})]$, a Leverett-type empirical function $K(s_{nw})$ appropriate for tested DM samples (presented by our group[19]) was implemented into the present approach. This empirical water retention function correlates the capillary pressure as a function of liquid saturation and PTFE content of the DM. At the final step, the benchmark data were categorized according to the different compressions and PTFE loadings of the DM and then integrated into a multidimensional linear regression model to deduce a representative semiempirical correlation describing the capillary pressure as a function of the relevant nondimensionalized experimental parameters. The general form of the capillary equation for the tested SGL 24 series DM samples is found as

$$P_C = \gamma\, 2^{0.4C}\sqrt{\frac{\varepsilon_c}{k}}K(s_{nw}) \quad [6]$$

Inserting the effective porosity and substituting the characteristic strain rate for SGL 24 series in terms of compression pressure, the final form of the characteristic capillary pressure correlation for SGL 24 series yields

$$P_C = \gamma\, 2^{0.4C}\left[\left(\frac{0.9}{1 + (-0.0083C^2) + (0.0911C)} + 0.1\right)\frac{\varepsilon_o}{k}\right]^{1/2}K(s_{nw}) \quad [7]$$

$$K(s_{nw}) = \begin{cases} (\text{wt }\%)[0.0469 - 0.00152(\text{wt }\%) - 0.0406s_{nw}^2 + 0.143s_{nw}^3] + 0.0561 \ln s_{nw} & 0 < s_{nw} \le 0.50 \\ (\text{wt }\%)[1.534 - 0.0293(\text{wt }\%) - 12.68s_{nw}^2 + 18.824s_{nw}^3] + 3.416 \ln s_{nw} & 0.50 < s_{nw} \le 0.65 \\ (\text{wt }\%)[1.7 - 0.0324(\text{wt }\%) - 14.1s_{nw}^2 + 20.9s_{nw}^3] + 3.79 \ln s_{nw} & 0.65 < s_{nw} < 1.00 \end{cases}$$

Similarly, substituting the compression stress-strain relationship (given in Eq. 5) of SGL 10BB DM, the final form of the modified capillary pressure function for SGL 10BB carbon paper becomes

$$P_C = \gamma\, 2^{0.4C}\left[\left(\frac{0.9}{1 + (-0.0046C^2) + (0.0843C)} + 0.1\right)\frac{\varepsilon_o}{k}\right]^{1/2}K(s_{nw}) \quad [8]$$

$$K(s_{nw}) = \begin{cases} (\text{wt }\%)[0.0469 - 0.00152(\text{wt }\%) - 0.0406s_{nw}^2 + 0.143s_{nw}^3] + 0.0561 \ln s_{nw} & 0 < s_{nw} \le 0.50 \\ (\text{wt }\%)[1.534 - 0.0293(\text{wt }\%) - 12.68s_{nw}^2 + 18.824s_{nw}^3] + 3.416 \ln s_{nw} & 0.50 < s_{nw} \le 0.65 \\ (\text{wt }\%)[1.7 - 0.0324(\text{wt }\%) - 14.1s_{nw}^2 + 20.9s_{nw}^3] + 3.79 \ln s_{nw} & 0.65 < s_{nw} < 1.00 \end{cases}$$

where (wt %), k, and s_{nw} are PTFE weight percentage, absolute permeability of the DM, and nonwetting liquid saturation, respectively. $K(s_{nw})$ represents the empirical Leverett function appropriate for the tested DM samples. It is worthwhile to re-emphasize that Eq. 7 and 8 are appropriate for SGL 24 series DM and SGL 10BB carbon papers at room temperature, respectively. Equations 7 or 8 can be modified to account for compression in any type of DM by implementing the characteristic compression-strain relation of the DM into the general form of the equation presented in Eq. 6.

Validation and comparison.— Figures 8 and 9 depict the comparison of the hydrophobic pore network capillary pressure predictions by the present empirical correlation (Eq. 7) and the standard Leverett approach (Eq. 2) with respect to the measured drainage capillary pressure at 1.4 MPa compression for SGL 24BC and SGL24DC carbon papers. As seen from Fig. 8 and 9, the presented modified approach generally predicts the capillary pressure well with small deviations observed in the saturation range of 0.50–0.70. This de-

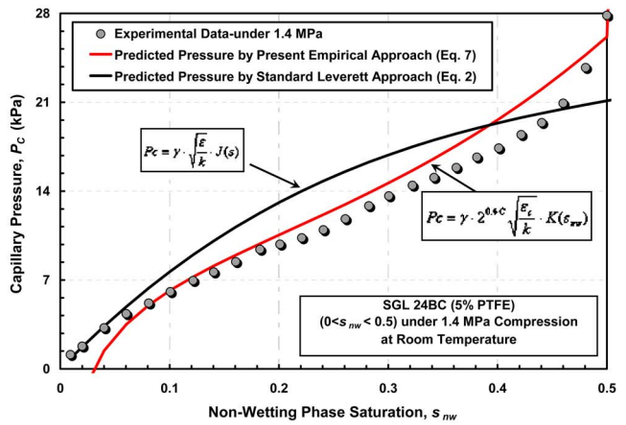

Figure 8. (Color online) Comparison of the present Leverett approach (given in Eq. 7), the standard Leverett approach (Eq. 2), and the experimental data for SGL 24BC under 1.4 MPa compression over a saturation range of (a) $0 < s_{nw} < 0.5$ and (b) $0 < s_{nw} < 1$.

viation likely stems from the complex shape of the capillary pressure-saturation curves. However, at high saturations ($s_{nw} > 0.70$), the present approach (Eq. 7) captures the change in capillary pressure and successfully predicts the measured capillary pressure within an uncertainty of +12% of the measured value. Overall, in the entire saturation domain ($0 < s_{nw} < 1$), the approach (Eq. 7) in the prescribed functional form predicts the capillary pressure with an uncertainty of ±15% of the measured capillary pressure. In contrast, the standard Leverett approach (Eq. 2) deviates enormously, nearly up to two orders of magnitude from the experimental data over the entire saturation domain, especially at high saturations ($s_{nw} > 0.5$), as clearly seen in Fig. 8 and 9. The present results also confirm that the standard Leverett approach equipped with the Leverett *J*-function appears to be incapable of tracking the changes in the capillary pressure due to the applied compression and the mixed wettability characteristics of the fuel cell DM.

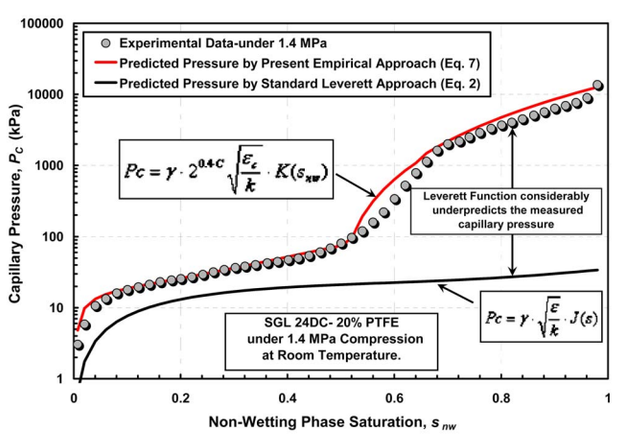

Figure 9. (Color online) Comparison of the present Leverett approach (given in Eq. 7), the standard Leverett approach (Eq. 2), and the experimental data for SGL 24DC (20% PTFE) under 1.4 MPa compression.

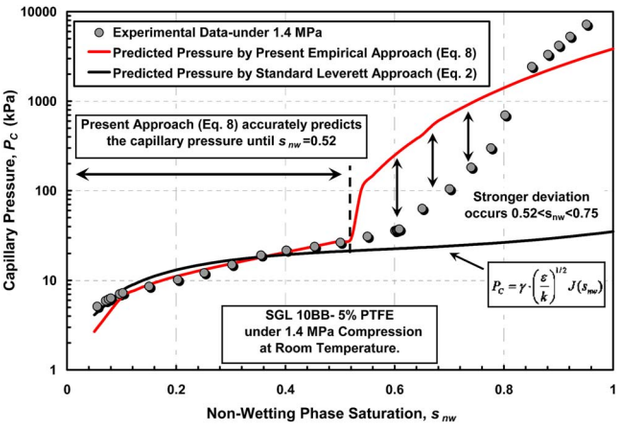

Figure 10. (Color online) Comparison of the present Leverett approach (given in Eq. 8), the standard Leverett approach (Eq. 2), and the experimental data for SGL 10BB (5% PTFE) under 1.4 MPa compression.

A further comparison between the predicted capillary pressure (by Eq. 8) and the measured capillary pressure of the hydrophobic pore network of SGL 10BB (5% PTFE) carbon paper was also performed to validate and evaluate the effectiveness of the present empirical Leverett approach. Additional stress-strain experiments were performed for SGL 10BB carbon substrate and the corresponding compressive strain-pressure relationship is given in Eq. 5. Using the appropriate functional form of the present Leverett approach (Eq. 8), the capillary pressure over a full spectrum of nonwetting saturation was predicted under 1.4 MPa compression. Figure 10 shows the experimental data and the capillary pressures predicted by using the present empirical approach (Eq. 8) and standard Leverett approach (Eq. 2) under 1.4 MPa compression at room temperature. As shown in Fig. 10, the present approach successfully approximates the capillary pressure up to saturation 0.52 (to within ±5.6%). As the saturation further increases, the predictions tend to exhibit a deviation from the experimental data, especially $0.52 < s_{nw} < 0.75$; however, the predictions recover the deviation to some extent at high saturations ($s_{nw} > 0.8$). The curve fit derived in the present work relies heavily on the SGL 24 series DM data; thus, for more accurate prediction of SGL 10BB, additional experiments would be required to develop a more generalized empirical correlation.

Finally, the drainage capillary pressure for the hydrophobic pore network of a DM treated with 5% PTFE content was predicted over a wide range of compressions by the present approach given in Eq. 7 (using the SGL 24 series strain-stress relationship) in order to validate and compare the effects of compression with the experimental observations. Figure 11 depicts the predicted capillary pressures vs nonwetting saturation under compressions of 0, 1, 2, and 3 MPa. For a specified saturation, the capillary pressure appears to increase with an increase in applied compression pressure, in good agreement with the experimental observations.

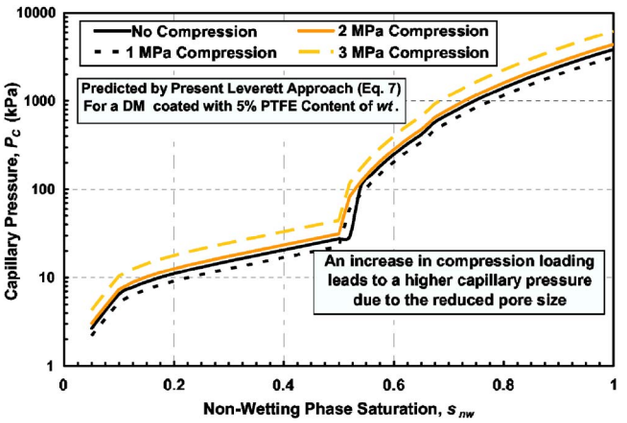

Figure 11. (Color online) Predicted capillary pressure (by the present empirical correlation given in Eq. 7) vs nonwetting saturation for a DM with 5% PTFE at different compressions.

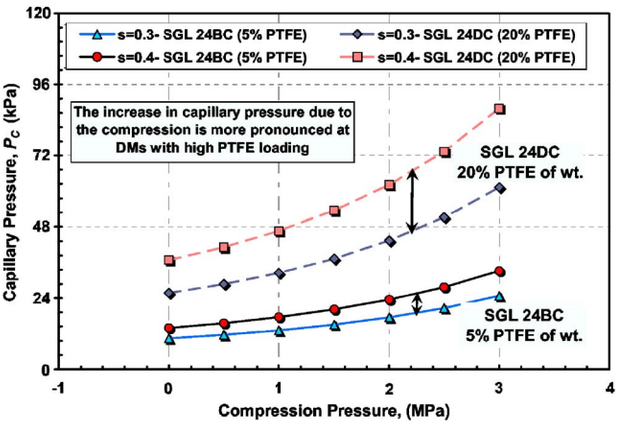

Figure 12. (Color online) The capillary pressure predicted by the present empirical approach (Eq. 7) vs compression pressure of SGL 24BC and SGL 24DC at specified saturations.

The key features of the generalized functional form of the presented empirical capillary pressure-saturation correlation (given in Eq. 6) are summarized as follows:

1. The present approach accurately predicts the measured capillary pressure with an uncertainty of ±15% of the measured values, showing considerable improvement over the traditional Leverett approach, which underpredicts the capillary pressure in the high-saturation region ($s_{nw} > 0.5$) by nearly two orders of magnitude.
2. The form of the capillary pressure-saturation equation accounts for the reduction in effective pore size by adjusting the effective porosity through the specific strain-stress relations of the DM.
3. The phase distributions over a wide range of hydrophobic content can be accurately captured by the well-defined empirical Leverett-type function (Eq. 7) given in the first phase of this paper series.[19]
4. The present empirical approach does not require any representative contact angle as an input, therefore overcoming a major limitation of the original Leverett approach. The variations in internal contact angle are implicitly embedded into the PTFE parameter (wt %) of the new Leverett function, therefore eliminating the need for the selection of a single (and unrealistic) surface contact angle.

It is worthwhile to emphasize that the present correlation given in Eq. 6 is derived based on the generated drainage data for the hydrophobic pore network of the DM samples coated with a microporous layer. Therefore, the porous media of interest herein is a composite structure. The capillary pressure-saturation curves of the DM macrosubstrate (without MPL) can be extracted from the overall behavior of the composite structure by using the corresponding the pore size distribution and porosities of the macro and microsubstrate (MPL). In other words, the characteristic capillary pressure-saturation relationship of the macro DM substrate (i.e., without MPL) can be determined from the given composite relationship in Eq. 6 by extending the capillary pressure-saturation trend of the composite DM from low saturation to high saturations, i.e., eliminating the MPL region, as discussed in Ref. 19.

Effect of PTFE and compression: coupled effect.— The engineering consequences of increasing PTFE content and compression should be systematically addressed in order to achieve the most favorable capillary transport characteristics and minimize the additional losses introduced by these parameters. In order to assess the relative significance of PTFE and compression on the capillary transport, the capillary pressure vs the compression pressure for SGL 24BC (5% PTFE) and SGL 24DC (20% PTFE) was predicted at constant water saturation values by the present empirical Leverett approach (Eq. 7) and the results are shown in Fig. 12. As shown in Fig. 12, SGL 24 DC (20 wt % PTFE) carbon paper appears to exhibit a larger increase in capillary pressure (from 40 to 90 kPa at $s = 0.4$) as the compression is increased from 0 to 3 MPa. However, the capillary pressure for SGL 24BC (5 wt % PTFE) seems to be increased to a lesser extent (from 12 to 21 kPa at $s = 0.4$) with the same amount increase in compression. In other words, the effect of compression on the capillary pressure is amplified by rendering the DM more hydrophobic. Physically, increasing the compression reduces the effective pore size, restricting the flow in a more confined space and rendering the DM more hydrophobic promotes the molecular imbalance at the phase interface, reducing the surface adhesion energy.

Conclusion

The effect of compression on the capillary transport characteristics of thin-film fuel cell DM was thoroughly examined for SGL series DM samples coated with MPL. The drainage capillary pressure-saturation measurements at different compressions (0, 0.6, and 1.4 MPa) were performed for SGL 24 series DM tailored with a range of mixed wettability (5–20 wt % PTFE). The corresponding changes in the morphological structure of the tested DM samples were probed and the water retention characteristics of tested DMs were addressed. Based on these benchmark data, the traditional Leverett approach was revised and a more appropriate form of Leverett approach (Eq. 6), which incorporates the mixed wettability characteristics of fuel cell DM and the specific effects of compression, was derived. A Leverett-type empirical function,[19] which precisely captures the changes in the phase saturation as a function of hydrophobic coating, was implemented in the present approach. The results show that the present empirical fit predicts the capillary pressure with an average uncertainty of ±15% of the measured values, whereas the traditional Leverett approach exhibits enormous deviation from the measured capillary pressure data (up to nearly two orders of magnitude), especially at high saturations, $s_{nw} > 0.5$.

The results show that the compression of the DM leads to an increase in capillary pressure within the compression range from 0 to 0.6 MPa. Any further increase in compression above 0.6 MPa appears to have relatively less effect on the capillary pressure possibly due to the relatively higher increase of the hydrophilic characteristics of the tested DM samples. The current results also indicate that rendering the DM more hydrophobic amplifies the compression effect, yielding a higher capillary pressure for the same saturation and compression, possibly because of the reduction in effective pore size and the enhanced molecular imbalance at the phase interface. Furthermore, the connected hydrophilic porosity is observed to decrease with an increase in compression, leading to a reduction in water retention capacity.

Note that the temperature is also a key factor affecting the transport mechanism but is beyond the scope of this study. This effect is thoroughly investigated in the succeeding publication.[20] Development of an advanced fuel cell model using the presented benchmark correlations is ongoing work in our laboratory and will be reported in succeeding publications.

Acknowledgments

This research is supported by National Science Foundation grant no. CTS-0414319. The authors thank Dr. Alex Sakars from Porotech, Ltd., for performing the MSP experiments.

The Pennsylvania State University assisted in meeting the publication costs of this article.

List of Symbols

C	compression pressure, MPa
k	permeability, m^{-2}
P_C	capillary pressure, Pascal
P_e	pore entry pressure, Pascal
r	pore radius, m
s_{TR}	compressive strain, unitless
V	volume, m^3
s	saturation, unitless
wt %	weight percentage of hydrophobic additive, unitless

Greek

ε	porosity, unitless
θ	contact angle, degree
γ	surface tension of water-air, N m^{-1}

Subscripts

c	compressed
g	gas
l	liquid
o	uncompressed
w	wetting phase
nw	nonwetting phase
wrc	water retention capacity

References

1. E. C. Kumbur, K. V. Sharp, and M. M. Mench, *J. Power Sources*, **168**, 156 (2007).
2. V. Gurau, M. J. Bluemle, E. S. De Castro, Y.-M. Tsou, J. A. Mann, and T. A. Zawodzinski, Jr., *J. Power Sources*, **160**, 1156 (2006).
3. M. C. Leverett, *Trans. Am. Inst. Min., Metall. Pet. Eng.*, **142**, 152 (1941).
4. K. S. Udell, *Int. J. Heat Mass Transfer*, **28**, 485 (1985).
5. U. Pasaogullari and C. Y. Wang, *J. Electrochem. Soc.*, **151**, A399 (2004).
6. J. H. Nam and M. Kaviany, *Int. J. Heat Mass Transfer*, **46**, 4595 (2003).
7. H. Ohn, T. V. Nguyen, D. Jacobson, D. Hussey, and M. Arif, *ECS Trans.*, **1**(6), 481 (2006).
8. S. Escribano, J.-F. Blachot, J. Etheve, A. Morin, and R. Mosdale, *J. Power Sources*, **156**, 8 (2006).
9. I. Nitta, T. Hottinen, O. Himanen, and M. Mikkola, *J. Power Sources*, **171**, 26 (2007).
10. T. Hottinen, O. Himanen, S. Karvonen, and I. Nitta, *J. Power Sources*, **171**, 113 (2007).
11. A. Bazylak, D. Sinton, Z. S. Liu, and N. Djilali, *J. Power Sources*, **163**, 784 (2007).
12. J. Ge, A. Higier, and H. Liu, *J. Power Sources*, **159**, 922 (2006).
13. J. P. Feser, A. K. Prasad, and S. G. Advani, *J. Power Sources*, **162**, 1226 (2006).
14. A. Vlahinos, K. Kelly, J. D'Aleo, and J. Stathopoulos, in *ASME 1st International Conference on Fuel Cell Science, Engineering, and Technology Conference*, ASME, p. 111 (2003).
15. Y.-H. Lai, D. P. Miller, C. Ji, and T. A. Trabold, in *ASME 1st International Conference on Fuel Cell Science, Engineering, and Technology Conference*, ASME, p. 567 (2003).
16. E. C. Kumbur, K. V. Sharp, and M. M. Mench, *J. Power Sources*, **161**, 333 (2006).
17. W.-K. Lee, C.-H. Ho, J. W. Van Zee, and M. Murthy, *J. Power Sources*, **84**, 45 (1999).
18. S.-J. Lee, C.-D. Hsu, and C.-H. Huang, *J. Power Sources*, **145**, 353 (2005).
19. E. C. Kumbur, K. V. Sharp, and M. M. Mench, *J. Electrochem. Soc.*, **154**, B1295 (2007).
20. E. C. Kumbur, K. V. Sharp, and M. M. Mench, *J. Electrochem. Soc.*, **154**, B1315 (2007).
21. Y. M. Volfkovich, V. S. Bagotzky, V. E. Sosenkin, and I. A. Blinov, *Colloids Surf., A*, **187–188**, 349 (2001).
22. A. Turhan, K. Heller, J. S. Brenizer, and M. M. Mench, *J. Power Sources*, **160**, 1195 (2006).
23. J. J. Kowal, A. Turhan, K. Heller, J. Brenizer, and M. M. Mench, *J. Electrochem. Soc.*, **153**, A1971 (2006).
24. N. R. Morrow, *Chem. Eng. Sci.*, **25**, 1799 (1970).
25. T. A. Corey, *Mechanics of Immiscible Fluids in Porous Media*, 1st ed., Water Resource Publications, Highlands Ranch, Co (1994).